Terahertz emission from a laser pulse with tilted front: Phase-matching versus Cherenkov effect

M. I. Bakunov,[1,2,a)] S. B. Bodrov,[2,1] and M. V. Tsarev[1,2]
[1]*University of Nizhny Novgorod, Nizhny Novgorod 603950, Russia*
[2]*Institute of Applied Physics, Russian Academy of Sciences, Nizhny Novgorod 603950, Russia*

(Received 12 March 2008; accepted 13 August 2008; published online 3 October 2008)

A theory that describes the terahertz generation via optical rectification of a femtosecond laser pulse with tilted front in an electro-optic crystal is developed. The theory accounts for the transverse size of the laser pulse and allows us to explore the dependence of the terahertz yield on laser focusing. Two typical experimental situations—$LiNbO_3$ excited with Ti:sapphire laser at room and cryogenic temperatures—are considered. It is shown that depending on temperature the dominant generation mechanism can be either phase-matching or Cherenkov effect. The parameters of the laser pulse (transverse size, tilt angle, and pulse duration) and crystal size maximizing the terahertz yield for $LiNbO_3$ are calculated. © *2008 American Institute of Physics*. [DOI: 10.1063/1.2989999]

I. INTRODUCTION

Optical rectification of ultrashort laser pulses in electro-optic crystals provides record optical-to-terahertz conversion efficiencies nowadays. This technique uses an optical pulse (pump) propagating through an electro-optic material to produce a nonlinear polarization that follows the intensity envelope of the pulse. The nonlinear polarization moves with the group velocity of the optical pulse and emits terahertz radiation.

The efficiency of the optical-to-terahertz conversion depends on the material parameters of the electro-optic crystal, such as its nonlinear coefficient, the velocity mismatch between the optical pulse and terahertz waves, and the coefficient of terahertz absorption. The presence of dispersion in the so-called subluminal materials,[1–3] in which the optical group velocity is smaller than the highest phase velocity for terahertz waves, gives rise to the existence of a frequency at which phase matching is achieved between the laser pulse and the terahertz wave propagating collinearly to the pulse. This provides a simple and effective way of terahertz generation: irradiation of a slab of subluminal material by a large (as compared to the terahertz wavelength) aperture beam of femtosecond laser pulses results in the phase-matched excitation of a quasiplane terahertz wave. For example, the optical rectification of Ti:sapphire laser pulses (~800 nm wavelength) in ZnTe, where phase matching with an ~2.5 THz wave occurs, is one of the most widely used methods for terahertz generation. However, the nonlinear coefficient of ZnTe is not as high as in some other materials, such as $LiNbO_3$, $LiTaO_3$, or DAST.[4] Moreover, a strong two-photon absorption of Ti:sapphire laser radiation in ZnTe at high laser intensities results in pump depletion and, what is even more essential, in the generation of free carriers that increase the terahertz absorption. These factors lead to saturation of terahertz yield at high laser intensities.

In the materials with higher optical nonlinearities and wider bandgaps (smaller multiphoton absorption), such as $LiNbO_3$ or $LiTaO_3$, the optical group velocity is about two times larger than the highest phase velocity of terahertz waves. In such materials, referred to as superluminal,[1–3] phase matching can be achieved in the Cherenkov configuration, i.e., between a strongly focused laser pulse and a plane terahertz wave propagating under a certain angle with respect to the laser path.[5–7] In this geometry the generated terahertz waves form a Cherenkov cone. The conical spatial distribution makes it difficult to collect the terahertz radiation for applications. A way to achieve the quasi-phase-matching conditions for large aperture laser beams is to use structures with periodically inverted sign of second-order susceptibility, such as periodically poled lithium niobate crystal[8,9] or orientation-patterned gallium arsenide.[10,11]

Another way to achieve phase-matching in a superluminal material is to use pump pulses with tilted fronts.[12] In such a pulse, the intensity front is tilted at a certain angle α with respect to the phase fronts. The pulse propagates with the optical group velocity V in the direction normal to the phase fronts; the projection of this velocity on the direction perpendicular to the intensity front is $V\cos\alpha$. By varying the tilt angle α, this projection can be made equal to the phase velocity of terahertz wave with an arbitrary frequency. Thus, a phase matching with the quasiplane terahertz wave propagating in the direction normal to the intensity front can be achieved. The operation principle has been demonstrated by generating subpicosecond pulses at approximately 2 THz from Ti:sapphire laser pulses in $LiNbO_3$ with a conversion efficiency of 4.3×10^{-5} at 77 K.[13] In less absorbing $LiNbO_3$ crystal compositions, the efficiency was increased up to 1.7×10^{-4} and tuning of the terahertz radiation between 1 and 4.4 THz by varying the tilt angle was demonstrated.[4] Further improvements of the conversion efficiency up to record values of $(5-7)\times10^{-4}$ at room temperature were reported in Refs. 14–16. Recently, the technique was extended to the conversion of Yb-laser pulses (1035 nm wavelength): using tilted-front pulses with duration of 300 fs and energy

a)Electronic mail: bakunov@rf.unn.ru.

400 μJ broadband (with a spectral bandwidth up to 2.5 THz) terahertz radiation was generated in $LiNbO_3$ with an efficiency of 2.5×10^{-4}.[17]

Despite the record optical-to-terahertz conversion efficiencies obtained using optical pulses with tilted fronts, the theory of terahertz emission from such pulses has still not been developed sufficiently. In Refs. 4 and 18, a simple one-dimensional (1D) model is used to calculate the terahertz field at the exit boundary of a nonlinear crystal. In this heuristic model, the terahertz field is not calculated via solving Maxwell's equations with the nonlinear source, but represented as a sum of plane waves arriving from different sections of the crystal. The amplitudes of the plane waves are not calculated rigorously and therefore, the results were given in arbitrary units. Moreover, the 1D model does not account for the transverse size of the pulse and it does not distinguish between a tilted-front pulse and a usual pulse with reduced group velocity. In addition to that, Refs. 4 and 18 do not consider the transmission of the terahertz fields generated inside the crystal through the exit boundary. This transmission requires a separate treatment because the usual Fresnel formulas need to be modified for the forced terahertz pulses.[19] Three-dimensional calculations of Ref. 20 do not include neither the presence of the crystal boundaries nor such important effects as dispersion and absorption of terahertz waves. Meanwhile, these effects play a key role for terahertz generation in the phase-matched regime.[3]

We set two goals in the paper. The first is to develop a rigorous theory of the terahertz emission from an optical pulse with tilted intensity front that includes all essential factors, such as finite transverse size of the optical pulse, material dispersion and absorption in the terahertz range, and the transmission of the generated terahertz fields through the crystal boundary. The second is to apply this theory to typical experiments with $LiNbO_3$ and to provide specific recommendations how to optimize the parameters of the optical pump and the crystal size to increase the efficiency of terahertz generation.

We consider a two-dimensional (2D) case when the pump optical pulse is infinite in one direction and has a finite width in the other direction. The 2D case does not require very bulky calculations as the three-dimensional case of focusing to a spot. At the same time, it allows us to study the effect of laser focusing on the conversion efficiency. In practice, focusing pump laser pulse into a line by a cylindrical lens is used to scale up the energy of the terahertz pulses created by optical rectification.[14] In the experiments with tilted-front pulses,[14,17] the pulses were also elongated in one dimension [the focal spot sizes on the crystal were 0.9×1.3 (Ref. 14) and 1×2 mm (Ref. 17)].

Using the Fourier-transform technique, we obtain and analyze the solution of Maxwell's equations for the terahertz fields emitted from an optical pulse with tilted front in an electro-optic crystal. We apply the general formulas to two typical experimental situations—$LiNbO_3$ excited with Ti:sapphire laser at room and cryogenic temperatures—that differ significantly in the coefficient of terahertz absorption. We calculate the terahertz radiation patterns in bulk $LiNbO_3$ crystal and study the terahertz emission from the crystal. In particular, we explore the dependence of the generated terahertz spectrum and energy on the parameters of the optical pump (laser transverse size, tilt angle, and pulse duration). The optimal pump parameters and crystal size maximizing the terahertz yield are pointed out.

The paper is organized as follows. In Sec. II, we discuss the dynamical stages of terahertz generation in an electro-optic crystal: transient processes near the entrance boundary of the crystal, emission inside the crystal, and transmission of the terahertz fields through the exit boundary to vacuum. In Sec. III, we study the terahertz emission from an optical pulse with tilted front in a bulk electro-optic crystal. We describe our theoretical model and basic equations in Sec. III A. A general solution of the equations using the Fourier-transform technique is given in Sec. III B. We analyze the radiated fields in the 1D limit of a planar optical pulse in Sec. III C and for a focused optical pulse using the stationary phase approach in Sec. III D. The results of 2D numerical calculations are given in Sec. III E. In Sec. IV, we study the transmission of the generated terahertz fields through the exit boundary of the crystal. The applicability of the usual Fresnel formulas is discussed in Sec. IV A in the planar approximation. In the general case of a focused optical pulse, the transmission formulas are derived in Sec. IV B. In Sec. V, we study the spectral-spatial distribution of the terahertz emission from the crystal and the dependence of the terahertz spectrum and energy on the parameters of the pump optical pulse. For 10 K, the results are compared to the experiments in Ref. 4 and calculations in Ref. 18. For 300 K, the results are compared to the experiments in Refs. 4 and 14. In the final Sec. VI we summarize our recommendations how to achieve efficient terahertz generation with tilted-front pulses and give concluding remarks.

II. DYNAMICAL STAGES OF TERAHERTZ GENERATION IN CRYSTALS

When an optical pulse enters an electro-optic crystal, the excited terahertz field can be described as a superposition of two terms: a forced-wave response that propagates with the velocity of the pump optical pulse (i.e., optical group velocity) and a free-wave response that propagates with the group velocity in the terahertz range.[3] Near the entrance boundary of the crystal the responses overlap and partially compensate each other; in the course of propagation they become separated and the total terahertz field increases. While the forced-wave response does not change in the course of propagation, the free-wave response changes in shape and reduces in amplitude, owing to the presence of dispersion and absorption. Physically, the forced-wave response is the near field of the nonlinear source and the waves excited owing to phase-matching with the source; the free-wave response is the transition radiation propagating from the entrance boundary of the crystal. In such crystals as $LiNbO_3$, terahertz absorption is significant (~20 cm^{-1} at 1 THz at room temperatures[4,21]) and the free-wave response decays fast (at a distance of ~1 mm in $LiNbO_3$ at room temperatures). Thus, it is the forced-wave response which is of interest from the practical point of view. In Sec. III, we study the stationary regime of

terahertz emission from a tilted-front pulse propagating in an infinite crystal, i.e., the forced-wave solution of Maxwell's equations with a nonlinear source.

The next stage of the generation process is the transmission of the generated terahertz fields through the exit boundary of the crystal to vacuum. The description of this stage is not as simple as it is often assumed in literature. Indeed, it is typically assumed that the terahertz fields generated by a pulse with nontilted-front experience transmission and reflection at the crystal boundary according to the usual Fresnel formulas (see, for example, Refs. 22–24). However, Ref. 19 showed that the commonly used Fresnel formulas are, in general, inapplicable to the forced terahertz pulses (the near field of moving nonlinear sources), and modified Fresnel formulas for the forced pulses were introduced. According to Ref. 19, the Fresnel formulas for the free and forced pulses differ significantly in strongly superluminal materials, such as $LiNbO_3$. In Sec. IV, this problem will be discussed for the terahertz fields created by optical pulses with tilted fronts.

III. TERAHERTZ EMISSION IN BULK CRYSTAL: GENERAL THEORY AND APPLICATION TO $LINBO_3$

A. Model and basic equations

We consider a homogeneous electro-optic crystal characterized by a one-phonon-resonance dielectric function in the terahertz range

$$\varepsilon = \varepsilon_\infty + \frac{(\varepsilon_0 - \varepsilon_\infty)\omega_{\mathrm{TO}}^2}{\omega_{\mathrm{TO}}^2 - \omega^2 + i\gamma\omega}, \tag{1}$$

where ε_0 and ε_∞ are the low and high frequency dielectric constants, respectively, ω_{TO} is the transverse optical phonon frequency, and γ is the damping rate. In our examples, we will use the following parameters for $LiNbO_3$:[4,25] $\omega_{\mathrm{TO}}/(2\pi)=7.44$ THz, $\varepsilon_0=26$, $\varepsilon_\infty=10$, and two damping rates $\gamma/(2\pi)=0.08$ and 2.3 THz for temperatures of 10 and 300 K, respectively. In practice, the parameters ω_{TO}, ε_0, and ε_∞ differ slightly for congruent and stoichiometric lithium niobate and depend to some extent on Mg-doping level and temperature.[21] We use typical values for these parameters. The damping rates are chosen to fit the experimental results of Ref. 21 for a 0.68 mol % stoichiometric $LiNbO_3$. In the optical range, the crystal is characterized by its phase refractive index n_{opt} and group refractive index n_g. It is assumed that $n_g^2 < \varepsilon_0$ (superluminal material[3]). For example, for a $LiNbO_3$ crystal excited with Ti:sapphire laser (~800 nm wavelength) we will use $n_{\mathrm{opt}}=2.16$ and $n_g=2.23$.[4]

We assume that a femtosecond laser pulse propagates in the crystal in the x-direction with group velocity $V=c/n_g$. The intensity front of the pulse is tilted at an angle α with respect to the phase fronts (Fig. 1). We neglect pulse depletion due to linear absorption (typically weak in such crystals as $LiNbO_3$) and multiphoton processes. The latter is a reasonable approximation at not very high pump intensities we are interested in here. Under these approximations, the nonlinear polarization induced in the crystal via optical rectification becomes

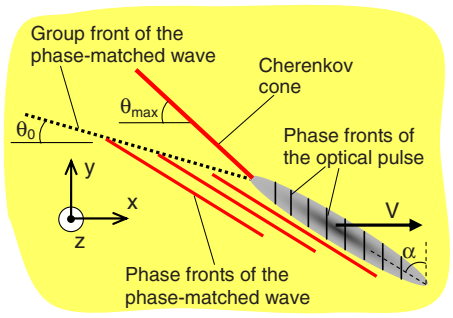

FIG. 1. (Color online) Schematics of an optical pulse with tilted intensity front and the radiation pattern produced by the pulse in an electro-optic crystal.

$$\mathbf{P}^{\mathrm{NL}} = \mathbf{p}F(\xi - y/V_y)G(y), \tag{2}$$

where the function $G(y)$ describes the transverse size of the optical beam; the function $F(\xi)$ is the time-dependent envelope of optical intensity, $\xi=t-x/V$, and $V_y=V\cot\alpha$. To specify our final formulas, we will use Gaussian functions

$$F(\xi) = e^{-\xi^2/\tau^2}, \quad G(y) = e^{-y^2/\ell_\perp^2}, \tag{3}$$

where τ is the pulse duration [the standard full width at half maximum (FWHM) is $\tau_{\mathrm{FWHM}}=2\sqrt{\ln 2}\tau$]. We will also use $\ell_{\perp\mathrm{FWHM}}=2\sqrt{\ln 2}\ell_\perp$. The orientation of the amplitude vector $\mathbf{p}$ is determined by the polarization of the optical pulse and orientation of the crystallographic axes of the sample. We assume typical experimental configurations: $p_x=p_y=0$ and $p_z\neq 0$.[4,14,17] For example, in perovskite materials, such as $LiNbO_3$ or $LiTaO_3$, the laser pulse is typically polarized along the optical axis (z-axis in our coordinate system) and produces nonlinear polarization in the same direction with $p_z=d_{33}E_0^2$, where d_{33} is the nonlinear coefficient and E_0 is the peak value of the optical field in the crystal. For $LiNbO_3$, we will use $d_{33}=166$ pm/V.[26]

To find the terahertz radiation generated by the moving nonlinear polarization (2), we use Maxwell's equations with the independent variables ξ and y

$$\frac{\partial E_z}{\partial y} = -\frac{1}{c}\frac{\partial B_x}{\partial \xi}, \tag{4a}$$

$$\frac{\partial}{\partial \xi}(E_z + n_g^{-1}B_y) = 0, \tag{4b}$$

$$-\frac{1}{V}\frac{\partial B_y}{\partial \xi} - \frac{\partial B_x}{\partial y} = \frac{1}{c}\frac{\partial D_z}{\partial \xi} + \frac{4\pi}{c}\frac{\partial P_z^{\mathrm{NL}}}{\partial \xi}. \tag{4c}$$

All formulas in the paper are in cgs units. These equations are supplemented by a constitutive relation between the displacement D_z and electric field E_z in the terahertz range. This relation can be conveniently written in the frequency domain using dielectric constant (1) (see Sec. III B).

B. General solution for the emitted terahertz field

To solve Eqs. (4a)–(4c), we apply Fourier transforms with respect to ξ and y and use the constitutive relation between the Fourier transforms of the electric field and displacement vector (ω and g are the Fourier variables which

correspond to ξ and y, respectively; $\tilde{}$ will denote quantities in the Fourier domain): $\tilde{D}_z(\omega,g)=\varepsilon(\omega)\tilde{E}_z(\omega,g)$, where the complex dielectric function $\varepsilon(\omega)$ is given by Eq. (1). Eliminating $\tilde{B}_x$ and $\tilde{B}_y$ using

$$\tilde{B}_x=(cg/\omega)\tilde{E}_z, \quad \tilde{B}_y=-n_g\tilde{E}_z, \tag{5}$$

we obtain

$$\tilde{E}_z(\omega,g)=\frac{4\pi p_z}{n_g^2-\varepsilon+c^2g^2/\omega^2}\tilde{F}(\omega)\tilde{G}(g-\omega/V_y). \tag{6}$$

In Eq. (6), we introduced the Fourier transforms $\tilde{F}(\omega)=(\tau/2\sqrt{\pi})e^{-\omega^2\tau^2/4}$ and $\tilde{G}(g)=(\ell_\perp/2\sqrt{\pi})e^{-g^2\ell_\perp^2/4}$ of the envelope $F(\xi)$ and beam profile $G(y)$, respectively.

With solutions (6) and (5) in the Fourier domain at hand, we can transform them to the ξ,y domain by taking inverse transforms such as

$$E_z(\xi,y)=\int_{-\infty}^{\infty}d\omega\int_{-\infty}^{\infty}dg\tilde{E}_z(\omega,g)e^{i\omega\xi-igy}. \tag{7}$$

C. Emission from a planar optical pulse

To get an analytical insight into the process of terahertz generation, we consider first the limiting case of a planar optical pulse $\ell_\perp\to\infty$. In this limit, the function $\tilde{G}(g-\omega/V_y)$ in Eq. (6) transforms to the delta function $\delta(g-\omega/V_y)$. Substitution of $\delta(g-\omega/V_y)$ into Eq. (7) gives

$$E_z(\xi,y)=4\pi p_z\int_{-\infty}^{\infty}d\omega\frac{\tilde{F}(\omega)e^{i\omega(\xi-y/V_y)}}{(n_g/\cos\alpha)^2-\varepsilon(\omega)}. \tag{8}$$

According to Eq. (8), the generated terahertz field in this limit depends only on the combination of variables $\eta=\xi-y/V_y$: $E_z(\xi,y)=E_z(\eta)$.

Integral (8) is similar to that describing the terahertz generation by an ordinary (nontilted) optical pulse but in a virtual medium with optical group refractive index $n_g/\cos\alpha$ (compare with Ref. 3). Varying the tilt angle α is equivalent to changing the optical group refractive index of the virtual medium and, thus, allows one to realize different regimes of terahertz generation. In particular, the tilt angle α can be made to satisfy the phase-matching condition $\varepsilon(\omega)-n_g^2/\cos^2\alpha=0$ (at $\gamma\to0$) at a selected terahertz frequency ω. In superluminal materials ($n_g^2<\varepsilon_0$) we are interested in here, the phase-matched frequency can be tuned in the whole interval $0<\omega<\omega_{TO}$ by varying the tilt angle within the interval $\alpha_{min}<\alpha<90°$, where α_{min} is given by

$$\cos\alpha_{min}=n_g/\sqrt{\varepsilon_0}. \tag{9}$$

We focus here only on the lower-frequency branch (below ω_{TO}) of phonon polaritons since the excitation of the higher-frequency branch (above the longitudinal optical phonon frequency ω_{LO}) requires very short optical pulses. Using the parameters of $LiNbO_3$ we obtain $\alpha_{min}\approx64.1°$.

Let us evaluate integral (8) analytically. For $\cos\alpha>n_g/\sqrt{\varepsilon_0}$, or $\alpha<\alpha_{min}$, the integrand in Eq. (8) has no singularities. Therefore, as a first approximation, we can neglect dispersion and absorption in the terahertz range and consider $\varepsilon(\omega)$ as a real constant ε_0 [more accurately, an additional condition on the pulse duration $\omega_{TO}^2\tau_{FWHM}^2\gg(\varepsilon_0-\varepsilon_\infty)[\varepsilon_0-(n_g/\cos\alpha)^2]^{-1}$ is required to avoid spectral distortion due to the frequency-dependent denominator in Eq. (8)]. This approximation gives

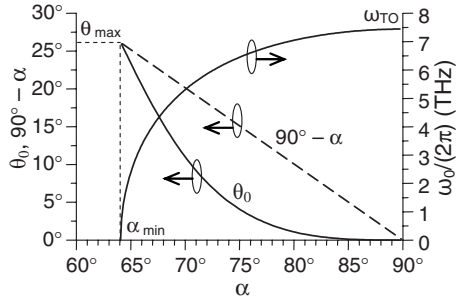

FIG. 2. The frequency ω_0 and the angles of the group (θ_0) and phase ($90°-\alpha$) fronts of the phase-matched terahertz wave as functions of α for $LiNbO_3$ with negligible damping excited with Ti:sapphire laser.

$$E_z(\eta)=\frac{4\pi p_z}{(n_g/\cos\alpha)^2-\varepsilon_0}F(\eta). \tag{10}$$

Equation (10) predicts the generation of a terahertz pulse of the Gaussian shape, which mimics the envelope of optical intensity. From the physical point of view, the generated terahertz pulse is the near field of the nonlinear source.

For $\cos\alpha<n_g/\sqrt{\varepsilon_0}$, i.e., for $\alpha>\alpha_{min}$, there is a singularity in the integrand in Eq. (8) and, therefore, dispersion cannot be neglected. Extending integration in Eq. (8) to the complex ω-plane, one can represent the solution as a sum of two terms: near field of the moving source and radiation behind the source. The latter is given by residue contributions from the poles defined by the equation $\varepsilon(\omega)-n_g^2/\cos^2\alpha=0$. Using Eq. (1) for $\varepsilon(\omega)$, we find the positions of the poles: $\omega=\pm\omega_0+i\gamma/2$, where

$$\omega_0=\omega_{TO}\sqrt{\frac{n_g^2-\varepsilon_0\cos^2\alpha}{n_g^2-\varepsilon_\infty\cos^2\alpha}-\frac{\gamma^2}{4\omega_{TO}^2}}, \tag{11}$$

and then calculate the residue contributions (for $\eta>0$)

$$E_z(\eta)=\frac{4\pi^{3/2}p_z\tau(\omega_{TO}^2-\omega_0^2-\gamma^2/4)^2}{\omega_0\omega_{TO}^2(\varepsilon_0-\varepsilon_\infty)}\times e^{-(\omega_0^2-\gamma^2/4)\tau^2/4}e^{-\gamma\eta/2}\sin[\omega_0(\eta-\gamma\tau^2/4)]. \tag{12}$$

Equation (12) describes a quasimonochromatic wavepacket propagating behind the optical pulse with velocity $V\cos\alpha$ in the normal direction to the intensity front of the pulse (at the angle α to the x-axis) and decaying with decrement $\gamma/(2V)$ with distance from the pulse.

The dependence of the frequency ω_0 on the tilt angle α for the parameters of $LiNbO_3$ and negligible damping ($\gamma\approx0$) is shown in Fig. 2. The curve is defined in the interval $\alpha_{min}<\alpha<90°$; damping, if included, slightly reduces α_{min}. Since in $LiNbO_3$ at room temperatures the terahertz absorption drastically increases at frequencies higher than 1–2 THz,[18] one can see from Fig. 2 that the most appropriate for terahertz generation is a narrow interval of the tilt angles

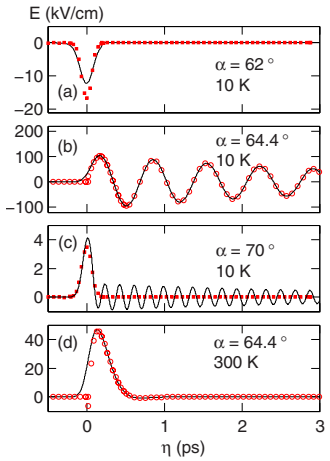

FIG. 3. (Color online) Total terahertz field (solid line), near field (filled squares), and phase-matched wave (open circles) plotted on the basis of Eqs. (8), (10), and (12), respectively, for different α (shown on the frames). Parameters used correspond to the excitation of $LiNbO_3$ with Ti:sapphire laser ($\tau_{FWHM}=150$ fs, $I_0=10$ GW/cm^2) at 10 K [(a)–(c)] and 300 K (d).

64.1°–65°. In cryogenically cooled $LiNbO_3$, due to significantly lower damping (see Ref. 18) higher frequencies can be generated at larger tilt angles.

According to Eq. (12), the optimal duration of the optical pulse, that maximizes the terahertz field magnitude, is given by $\tau\sqrt{\omega_0^2-\gamma^2/4}=\sqrt{2}$, or $\omega_0\tau\approx\sqrt{2}$ for small damping. However, the optimal pulse duration is relevant only to the case when p_z is independent of τ, i.e., for a fixed optical intensity. For a fixed energy of the optical pulse, $p_z\tau=$const in Eq. (12) and thus, τ affects the terahertz field magnitude only via the Gaussian factor. Thus, shortening of the optical pulse increases the generated terahertz field. This increase, however, saturates at $\tau<\omega_0^{-1}$ (for example, at $\tau<75$ fs, or $\tau_{FWHM}<125$ fs, for $\omega_0=2$ THz). Since the length of the terahertz wavepacket is independent of τ, the terahertz energy also depends on τ only via the Gaussian factor and saturates at $\tau<\omega_0^{-1}$. For a practically interesting case $\omega_{TO}^2\gg\omega_0^2,\gamma^2/4$ and optimal pump pulse duration $\tau<\omega_0^{-1}$, the amplitude of the generated terahertz wave is inversely proportional to its frequency: $E_z\propto\omega_0^{-1}$.

For $\omega_0\tau\gg1$, the amplitude of phase-matched wave (12) is small. Mathematically, the Gaussian factor $\tilde{F}(\omega)$ with relatively large values of τ brings to naught the integrand in Eq. (8) at the poles $\pm\omega_0+i\gamma/2$. Thus, the residue contributions of the poles become negligible. In this case, the denominator in Eq. (8) may be approximated by a constant and we arrive again at Eq. (10) that defines the near field of the nonlinear source.

Figure 3 shows oscillograms of $E_z(\eta)$ calculated by taking integral (8) numerically (solid line) or applying the approximate formulas (10) (filled squares) and (12) (open circles). The oscillograms are plotted for two values of γ and different α. We used the parameters of $LiNbO_3$ excited with Ti:sapphire laser at 10 K [Figs. 3(a)–3(c)] and 300 K [Fig. 3(d)]. The peak optical intensity $I_0=(c/8\pi)n_{opt}E_0^2$ was 10 GW/cm^2 and pulse duration was $\tau_{FWHM}=150$ fs.

For both 10 and 300 K, the generated terahertz field is described well by Eq. (12) for the phase-matched wave if α is just above $\alpha_{min}\approx64.1°$. In a narrow interval $64.1°<\alpha\leq66°$, according to our analysis, the near field is negligible [Figs. 3(b) and 3(d)]. For low damping (at 10 K), the phase-matched wave decays slowly with η [Fig. 3(b)]. For high damping (at 300 K), the phase-matched wave is overdamped—its attenuation length is smaller [Fig. 3(d)] than or comparable to the wavelength. Essentially, for a fixed $\alpha=64.4°$ the amplitude is reduced by a factor of 2 with temperature increase from 10 to 300 K [compare Fig. 3(b) with Fig. 3(d)].

For $\alpha<64.1°$ there is no phase-matched wave, and the terahertz field is described well by Eq. (10) for the near field if α is not too close to 64.1° [Fig. 3(a)]. For $\alpha>66°$, the amplitude of the phase-matched wave becomes small and the main peak of the terahertz field is also described well by Eq. (10) [Fig. 3(c)].

D. Emission from a focused optical pulse in the far field zone

For an arbitrary transverse size of the optical pulse, the integration contour for the inner integral on g of Eq. (7) is closed in the lower half plane of the complex g-plane for $y>0$ and in the upper half plane for $y<0$. The contours are similar to that of Refs. 27 and 28, but without branch cuts. The residue contributions to the integral from the poles given by $(g+\omega/V_y)^2-(\omega/c)^2[\varepsilon(\omega)-n_g^2]=0$ define the free space radiation; the contributions from the semi-infinite straight lines tilted at an angle of 45° with the axes (see Refs. 27 and 28) give the near field of the moving source. Thus, the total terahertz field consists of both the near field and the free space radiation. Taking into account only the residue contributions and, thus, neglecting the near field, we obtain (assuming for simplicity $\gamma=0$)

$$E_z(\xi,y)=\frac{8\pi^2p_z}{c^2}\int_0^{\omega_{TO}}d\omega\frac{\omega^2}{g}\tilde{F}(\omega)\tilde{G}\left(g\pm\frac{\omega}{V_y}\right)\times\sin(\omega\xi-g|y|), \tag{13}$$

with $g=(\omega/c)[\varepsilon(\omega)-n_g^2]^{1/2}$, "+" taken for $y<0$, and "–" for $y>0$. We again do not include the higher-frequency branch of phonon polaritons.

Integral (13) can be evaluated asymptotically for large ξ using the stationary phase method

$$E_z(\xi,y)\approx\frac{8\pi^{5/2}p_z\omega_s^2\tilde{F}(\omega_s)\tilde{G}(g_s\pm\omega_s/V_y)}{g_s|g_s''y|^{1/2}c^2}\times\sin\left[\omega_s\xi-g_s|y|-\frac{\pi}{4}\mathrm{sgn}(g_s'')\right], \tag{14}$$

where g_s'' denotes the second derivative with respect to ω taken at the frequency ω_s for which

$$V\frac{dg}{d\omega}=\frac{V\xi}{|y|}=\cot\theta, \tag{15}$$

where θ is the half-apex angle of the cone with apex on the moving laser pulse $\xi=0$.

Equation (15) is similar to that obtained and analyzed in Refs. 2 and 3 for an ordinary (nontilted) optical pulse propa-

gating in an electro-optic medium. In particular, this equation defines the angle $\theta_{\max}$ of the overall Cherenkov cone produced by the optical pulse and angular distribution of the terahertz frequency inside the cone. According to Refs. 2 and 3, in a superluminal material ($n_g^2 > \varepsilon_0$), the maximum cone angle corresponds to zero frequency and equals

$$\sin\theta_{\max} = n_g/\sqrt{\varepsilon_0}. \tag{16}$$

For example, for $LiNbO_3$ Eq. (16) gives $\theta_{\max} \approx 26°$. Inside Cherenkov cone (16), the frequency grows with decreasing θ, $\omega \to \omega_{TO}$ at $\theta \to 0$. For the excitation by a pulse with tilted front, Eqs. (9) and (16) give $\sin\theta_{\max} = \cos\alpha_{\min}$, i.e., $\theta_{\max}$ is the complementary angle to $\alpha_{\min}$: $\theta_{\max} + \alpha_{\min} = 90°$. The physical meaning of the relation $\theta_{\max} + \alpha_{\min} = 90°$ can be easily understood. Indeed, the Cherenkov radiation from a superluminal source may be considered as a superposition of partial plane waves of different frequencies ω propagating at different angles θ [see Eq. (13)]. The opening angle $\theta_{\max}$ of the overall Cherenkov cone corresponds to the partial plane wave with $\omega \to 0$ and the highest phase velocity $c/\sqrt{\varepsilon_0}$, partial plane waves with larger frequencies have lower phase velocities and propagate at smaller angles $\theta < \theta_{\max}$. For efficient excitation of a given frequency component, the intensity front of the optical pulse should be parallel to the phase front of the component: $\alpha = 90° - \theta$. Thus, the minimal α, for which the phase matching with a frequency component can be achieved, is defined by the maximal value of θ: $\alpha_{\min} = 90° - \theta_{\max}$.

The excitation with tilted-front pulses has several peculiarities which are related to the presence of the factor $\tilde{G}(g_s \pm \omega_s/V_y)$ in Eq. (14). First, the amplitude of the terahertz field inside the Cherenkov cone is asymmetric with respect to the laser path: the field is stronger for $y > 0$ and weaker for $y < 0$. Second, the maximum of $\tilde{G}(g_s \pm \omega_s/V_y)$, reached at $y > 0$ and $g_s - \omega_s/V_y = 0$, defines an angle θ_0 at which the group front of the phase-matched terahertz wave propagates. Indeed, the equality $g_s - \omega_s/V_y = 0$ is fulfilled for $\omega_s = \omega_0$, where ω_0 is the phase-matched frequency given by Eq. (11) at $\gamma = 0$. Substituting ω_0 into Eq. (15) gives the angle θ_0 for the group front of the phase-matched wave

$$\cot\theta_0 = \tan\alpha + \frac{\cot\alpha}{n_g^2(\varepsilon_0 - \varepsilon_\infty)}\left(\frac{n_g^2}{\cos^2\alpha} - \varepsilon_\infty\right) \times\left(\frac{n_g^2}{\cos^2\alpha} - \varepsilon_0\right). \tag{17}$$

The dependence of θ_0 on α is shown in Fig. 2. The phase fronts of the phase-matched wave are, naturally, parallel to the intensity front of the pump optical pulse, i.e., inclined at the angle $90° - \alpha$ to the laser path [see Eq. (14) and Fig. 1].

For $\alpha = \alpha_{\min}$, Eq. (17) is reduced to $\cot\theta_0 = \tan\alpha_{\min} = \cot\theta_{\max}$ or $\theta_0 = 90° - \alpha_{\min} = \theta_{\max}$. Thus, in this case the group front of the phase-matched wave, its phase fronts, and the Cherenkov cone are parallel each other and also to the intensity front of the pump optical pulse. For $\alpha > \alpha_{\min}$, according to Eqs. (17) and (16) all three angles are different: $\theta_0 < 90° - \alpha < \theta_{\max}$ (Fig. 2).

If the phase-matched wave is not excited ($\alpha < \alpha_{\min}$) or its group front and the Cherenkov cone are well separated in space (i.e., α exceeds significantly, by a few degrees for $LiNbO_3$, $\alpha_{\min}$), the structure of the Cherenkov cone can be described in the dispersionless approximation: $\varepsilon(\omega)$ can be approximated (under an additional condition of $\omega_{TO}\tau_{FWHM} \gg 1$) by ε_0 and integral (13) can be evaluated analytically

$$E_z(\xi, y) = -\frac{2\pi^{3/2} p_z \ell_\perp \tau}{c\tau_\pm(\varepsilon_0 - n_g^2)^{1/2}}\frac{d}{d\zeta}F(\zeta, \tau_\pm). \tag{18}$$

In Eq. (18), $F(\zeta, \tau_\pm)$ is the Gaussian function (3) with $\zeta = \xi - (|y|/c)(\varepsilon_0 - n_g^2)^{1/2}$ [a coordinate across Cherenkov cone (16)] used instead of ξ and $\tau_\pm = [\tau^2 + (\ell_\perp n_g/c)^2(\tan\alpha \pm \tan\alpha_{\min})^2]^{1/2}$ used instead of τ for $y < 0$ and $y > 0$, respectively. According to Eq. (18), the field distribution across Cherenkov cone (16) is given by the derivative of the optical pulse intensity envelope, similarly to the case of a nontilted-front pulse.[3] For the excitation with a tilted-front pulse, however, the effective characteristic time $\tau_\pm$ of the Gaussian function $F(\zeta, \tau_\pm)$ and, therefore, the cone's thickness differ for $y < 0$ and $y > 0$—the terahertz field distribution across the cone is smoother for $y < 0$ than for $y > 0$. The maximum value of the terahertz field at the Cherenkov cone

$$|E_z|_{\max} = \frac{(2\pi)^{3/2} p_z \ell_\perp \tau}{c\tau_\pm^2(\varepsilon_0 - n_g^2)^{1/2}} e^{-1/2}, \tag{19}$$

which is reached at $\zeta = \pm\tau_\pm/\sqrt{2}$, is smaller for $y < 0$ than for $y > 0$. The asymmetry of the radiation pattern is the most pronounced for $\alpha \approx \alpha_{\min}$, when $\tau_- \approx [\tau^2 + (\ell_\perp \varepsilon_0/cn_g)^2(\alpha - \alpha_{\min})^2]^{1/2}$ and $\tau_+ \approx [\tau^2 + 4(\ell_\perp/c)^2(\varepsilon_0 - n_g^2)]^{1/2}$, at an additional condition $\ell_\perp \gg c\tau$. For example, for weakly focused optical pulses with $\ell_{\perp FWHM} \sim 1$–2 mm, $\tau_{FWHM} \sim 150$–300 fs, and $\alpha \approx \alpha_{\min}$, that were used in Refs. 14 and 17, τ_+ is estimated as ~ 200 times larger than τ_-. Therefore, the $y < 0$ segment of the Cherenkov cone is negligible and the cone should be strongly asymmetric in these experiments.

For a fixed energy of the optical pulse, we have $p_z \ell_\perp \tau = \text{const}$ in Eq. (19) and $|E_z|_{\max} \propto \tau_-^{-2}$ (we consider only the practically interesting segment of the Cherenkov cone at $y > 0$). For a large $\ell_\perp$, even a small detuning α from $\alpha_{\min}$ can lead to a significant, as compared to τ, value of the term $(\ell_\perp n_g/c)|\tan\alpha - \tan\alpha_{\min}|$ in τ_-. For example, for the parameters of $LiNbO_3$ and $\ell_\perp = 1$ mm this term is $\sim 680|\alpha° - \alpha°_{\min}|$ fs, where the angles are expressed in degrees. Thus, even for $|\alpha° - \alpha°_{\min}| \sim 1°$ the square of this term exceeds significantly τ^2, with a typical value $\tau \sim 150$ fs, in τ_-. We can therefore conclude that for given τ and α a decrease in $\ell_\perp$ leads to an increase in $|E_z|_{\max}$; however, when $\ell_\perp$ becomes smaller than $(c\tau/n_g)|\tan\alpha - \tan\alpha_{\min}|^{-1}$, further focusing adds little to the terahertz field magnitude on the Cherenkov cone. Similarly, for given $\ell_\perp$ and α, a decrease in τ leads to an increase in $|E_z|_{\max}$ until τ becomes smaller than $(\ell_\perp n_g/c)|\tan\alpha - \tan\alpha_{\min}|$.

If we fix the optical intensity rather than its energy ($p_z = \text{const}$) and also fix $\ell_\perp$ and α in Eq. (19), then

$|E_z|_{\max} \propto \tau/\tau_-^2$. Therefore, there is an optimal pulse duration $\tau_{\text{opt}}=(\ell_\perp n_g/c)|\tan\alpha-\tan\alpha_{\min}|$ that maximizes $|E_z|_{\max}$ to $(2/e)^{1/2}\pi^{3/2}p_z/[n_g|\tan\alpha-\tan\alpha_{\min}|(\varepsilon_0-n_g^2)^{1/2}]$. If τ is fixed instead of $\ell_\perp$, then $|E_z|_{\max} \propto \ell_\perp/\tau_-^2$ and there is an optimal transverse size $\ell_{\perp\text{opt}}=(c\tau/n_g)|\tan\alpha-\tan\alpha_{\min}|^{-1}$ that maximizes $|E_z|_{\max}$ to the same value.

We can conclude here that the spectrum of the Cherenkov radiation $\propto p_z\ell_\perp\tau\omega\exp(-\omega^2\tau_-^2/4)$ [see Eq. (13)] has a maximum $\propto p_z\ell_\perp\tau\tau_-^{-1}$ at $\omega\tau_-=\sqrt{2}$; the position and magnitude of the maximum depend on all three parameters (τ, $\ell_\perp$, and α) of the optical pulse.

A weak absorption, described by Eq. (1) with $\gamma \ll \omega_{\text{TO}}$, can be incorporated into Eq. (18) by substitution

$$\tau_\pm \to \left[\tau_\pm^2 + \frac{2\gamma(\varepsilon_0-\varepsilon_\infty)|y|}{\omega_{\text{TO}}^2 c(\varepsilon_0-n_g^2)^{1/2}}\right]^{1/2}. \tag{20}$$

According to Eqs. (18)–(20), this absorption results in a gradual fading of the terahertz field at the Cherenkov cone and spreading of the field across the cone with the distance $|y|$. The size of the Cherenkov cone in the transverse direction becomes

$$|y|_{\max} \sim \frac{\omega_{\text{TO}}^2\tau_\pm^2 c(\varepsilon_0-n_g^2)^{1/2}}{2\gamma(\varepsilon_0-\varepsilon_\infty)}, \tag{21}$$

and its length is $L_{\text{Ch}}=|y|_{\max}/\sin\theta_{\max}$.

E. Emission from a focused optical pulse at arbitrary distances

Figure 4 shows the spatial distribution of the electric field E_z, calculated numerically on the basis of Eqs. (6) and (7), for several tilt angles and two damping rates. In the calculations, we used the parameters of $LiNbO_3$ excited with Ti:sapphire laser at 10 and 300 K. The parameters of the optical pulse were typical for experiments: $\tau_{\text{FWHM}}=150$ fs, $\ell_{\perp\text{FWHM}}=1$ mm, and $I_0=10$ GW/cm^2.

The radiation patterns presented in Fig. 4 can be interpreted using the analytical results of Secs. III C and III D. For a cryogenically cooled $LiNbO_3$ [Figs. 4(a)–4(c)] the characteristic features of the excitation with tilted-front pulses are well pronounced. For $\alpha<\alpha_{\min}$ [$\alpha=62°$ in Fig. 4(a), $\alpha_{\min}\approx 64.1°$], the generated terahertz field consists of the near field, which is localized in the region of the nonlinear source, and the asymmetric Cherenkov cone [the lower, at $y<0$, part of the cone is indiscernible in Fig. 4(a) because of its weakness, see Eq. (19)]. The opening angle of the Cherenkov cone $\theta_{\max}$ is about 26°, in accordance with Eq. (16). The electric field at the cone varies in the normal to the cone direction as the first derivative of the optical pulse intensity envelope, i.e., it consists of two adjacent pulses of opposite polarities, according to Eq. (18).

For $\alpha>\alpha_{\min}$ [Figs. 4(b) and 4(c)], the phase-matched wave appears in the radiation pattern. In Fig. 4(b), where $\alpha=64.4°$ and, thus, α exceeds $\alpha_{\min}$ only slightly, the group front of the phase-matched wave practically coincides with the Cherenkov cone [$\theta_0\approx\theta_{\max}$ according to Eq. (17), see also Fig. 2] and the wave manifests itself as the oscillating tail behind the Cherenkov cone. The frequency of the oscillations is about 1.5 THz, in accordance with Eq. (11) and

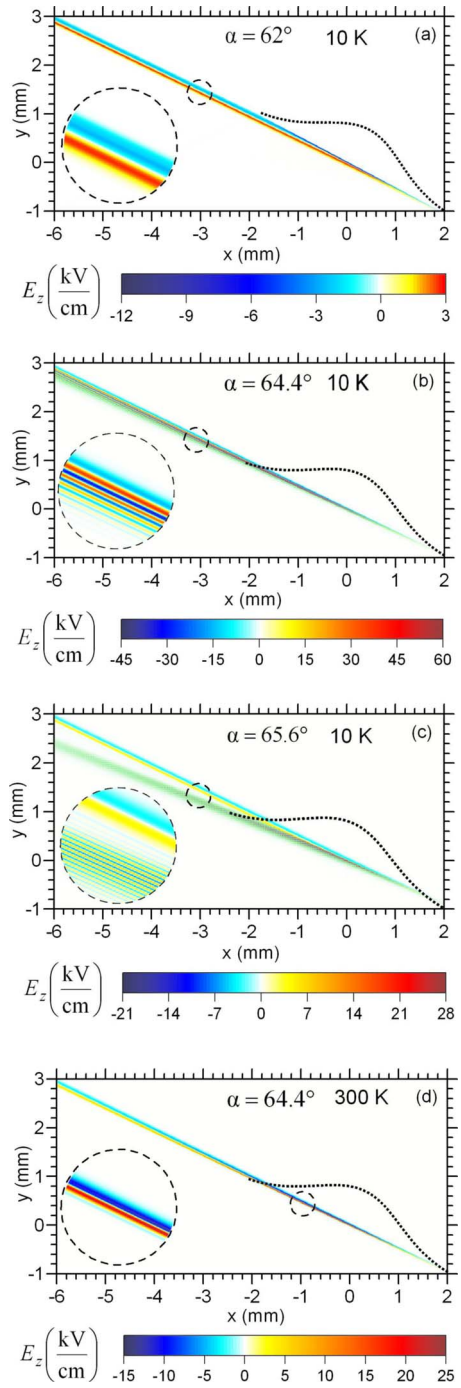

FIG. 4. (Color online) Snapshots of the electric field $E_z(x,y,t)$ produced in $LiNbO_3$ with Ti:sapphire laser ($\tau_{\text{FWHM}}=150$, $\ell_{\perp\text{FWHM}}=1$ mm, and $I_0=10$ GW/cm^2). The temperature and α are shown on the frames. The dotted line shows the transverse profile of the optical intensity.

Fig. 2. The generated terahertz fields are more than an order of magnitude stronger as compared to those in Fig. 4(a). For $\alpha=65.6°$ [Fig. 4(c)], the group front of the phase-matched wave and the Cherenkov cone are well separated [$\theta_{\max}-\theta_0\approx 5°$, in accordance with Eq. (17) and Fig. 2]. The frequency of the phase-matched wave is about 3 THz (see Fig. 2). The magnitude of the generated terahertz field is reduced by approximately a factor of two as compared to Fig. 4(b).

It is interesting to compare the terahertz field distribution across the Cherenkov cone in Figs. 4(a)–4(c). In Figs. 4(a)

and 4(c), the distribution is smoother and the field is weaker than in Fig. 4(b). It can be explained by larger values of the effective characteristic time τ_- for Figs. 4(a) and 4(c) than for Fig. 4(b) [see Eqs. (18) and (19)].

Focusing on the radiation pattern for the room temperature and $\alpha=64.4°$ [Fig. 4(d)], three essential features can be noted. First, the phase-matched wave is practically not excited. The magnitude of the generated terahertz fields in Fig. 4(d) is approximately half of those in Fig. 4(b). It agrees well with the predictions of the 1D model [see Figs. 3(b) and 3(c)]. Second, the Cherenkov cone at 300 K fades more rapidly with distance from the pump laser pulse than for 10 K. It agrees with Eq. (21). Third, even for $\ell_\perp$ much larger than the generated terahertz wavelength ($\ell_{\perp \mathrm{FWHM}}=1$ mm), the terahertz field in the region of the source is about half of the value predicted using the planar approximation for the pump pulse [Fig. 3(d)]. However, we verified that this approximation becomes more accurate with increasing $\ell_\perp$ and provides a good agreement with the numerical results for $\ell_{\perp \mathrm{FWHM}} > 5$ mm.

IV. TRANSMISSION THROUGH THE CRYSTAL BOUNDARY

In Secs. III A–III E we calculated and analyzed the terahertz fields generated by an optical pulse with tilted front inside an electro-optic crystal. Let us study now the transmission of the generated fields to vacuum at the exit boundary of the crystal. We assume that the exit boundary of the crystal is parallel to the intensity front of the pump optical pulse as in typical experiments.[4,14,17] We start with the planar approximation for the optical pulse. This allows us to focus on the key features of the boundary problem and compare our results with the 1D analysis of Ref. 19 for nontilted-front pulses.

A. Transmission formulas for a planar optical pulse

In the planar approximation, the terahertz field incident on the crystal boundary is given by Eq. (8). To solve the boundary problem, it is convenient to change variables x,y in Eq. (8) to new coordinates x' (normal to the boundary) and y' (tangential to the boundary): $x=x'\cos\alpha - y'\sin\alpha$, $y=x'\sin\alpha + y'\cos\alpha$. In the coordinates x',y' a Fourier component of the incident field with spatial dependence $\propto \exp[-i\omega n_g x'/(c\cos\alpha)]$ will produce a reflected component $\propto R\exp[i\omega\sqrt{\varepsilon(\omega)}x'/c]$ and a transmitted component $\propto T\exp(-i\omega x'/c)$. Matching the components by the boundary conditions of continuity of E_z and $\partial E_z/\partial x'$ at $x'=0$ gives the reflection and transmission coefficients R and T

$$R=\frac{n_g/\cos\alpha-1}{\sqrt{\varepsilon(\omega)}+1},\quad T=\frac{n_g/\cos\alpha+\sqrt{\varepsilon(\omega)}}{\sqrt{\varepsilon(\omega)}+1}. \tag{22}$$

The terahertz field transmitted to vacuum is given by the inverse Fourier integral

$$E_z^{(t)}(t,x')=4\pi p_z\int_{-\infty}^{\infty}d\omega\frac{T\tilde{F}(\omega)e^{i\omega(t-x'/c)}}{(n_g/\cos\alpha)^2-\varepsilon(\omega)}. \tag{23}$$

The reflected wave can be found from Eq. (23) by replacing $T\to R$ and $\exp[i\omega(t-x'/c)]\to\exp[i\omega(t+x'\sqrt{\varepsilon(\omega)}/c)]$.

The reflection and transmission coefficients R and T given by Eq. (22) differ from the usual Fresnel coefficients

$$R_F=\frac{\sqrt{\varepsilon(\omega)}-1}{\sqrt{\varepsilon(\omega)}+1},\quad T_F=\frac{2\sqrt{\varepsilon(\omega)}}{\sqrt{\varepsilon(\omega)}+1} \tag{24}$$

by the presence of the parameter $n_g/\cos\alpha$ that defines the group velocity of the optical pulse in the normal direction to its intensity front. In principle, using coefficients (22) instead of coefficients (24) should lead to nonconservation of the electromagnetic energy at the exit boundary due to work of the nonlinear polarization on the terahertz field.[19] This effect is, however, absent for the phase-matched wave at ω_0 excited when $\alpha>\alpha_{\min}$: for this wave $n_g/\cos\alpha=\sqrt{\varepsilon(\omega_0)}$ and, therefore, $R(\omega_0)=R_F(\omega_0)$, $T(\omega_0)=T_F(\omega_0)$. For the frequency components that describe the near field of the moving nonlinear source, i.e., for $\omega\neq\omega_0$ at $\alpha>\alpha_{\min}$ or for the whole spectrum at $\alpha<\alpha_{\min}$, the difference between the coefficients R,T and R_F,T_F becomes insignificant: $R(\omega)\approx R_F(\omega)$, $T(\omega)\approx T_F(\omega)$, if $\alpha\approx\alpha_{\min}$ and $\omega_{\mathrm{TO}}\tau_{\mathrm{FWHM}}\gg 1$. The condition $\alpha\approx\alpha_{\min}$ provides that $n_g/\cos\alpha\approx\sqrt{\varepsilon_0}$ [see Eq. (9)] and the condition $\omega_{\mathrm{TO}}\tau_{\mathrm{FWHM}}\gg 1$ bounds the generated terahertz spectrum to frequencies $\omega\ll\omega_{\mathrm{TO}}$ for which $\varepsilon(\omega)\approx\varepsilon_0$. Thus, unlike the excitation with nontilted-front pulses,[19] using the usual Fresnel formulas at the exit boundary of $LiNbO_3$ does not lead to significant errors in the practically interesting case realized at $\alpha\approx\alpha_{\min}$ and $\tau_{\mathrm{FWHM}}\gg 25$ fs. To keep our results more accurate, however, we will use the accurate formula for the transmission coefficient in our analysis of the energetics of terahertz emission from finite aperture optical pulses (see Sec. V).

B. Transmission formulas for a focused optical pulse

In the general case of a finite aperture pump optical pulse, we take the incident on the boundary terahertz field in the form given by Eqs. (6) and (7). We solve the boundary problem in the Fourier domain again using the coordinates x',y' and the boundary conditions of continuity of E_z and $\partial E_z/\partial x'$. This gives the reflection and transmission coefficients for a Fourier component of frequency ω

$$R=[\omega n_g(c\cos\alpha)^{-1}-h_t'+g'\tan\alpha](h_r'+h_t')^{-1}, \tag{25a}$$

$$T=[\omega n_g(c\cos\alpha)^{-1}+h_r'+g'\tan\alpha](h_r'+h_t')^{-1}, \tag{25b}$$

where $g'=g\cos\alpha-(\omega n_g/c)\sin\alpha$ is the tangential to the boundary wave vector (same in the incident, reflected, and transmitted waves), and $h_r'=(\omega/c)[\varepsilon(\omega)-c^2g'^2/\omega^2]^{1/2}$ and $h_t'=(\omega/c)(1-c^2g'^2/\omega^2)^{1/2}$ are normal to the boundary wave vectors of the reflected and transmitted Fourier components, respectively. The transmitted to vacuum terahertz field can be written as

$$E_z^{(t)}(t,x',y') = \frac{1}{\cos\alpha}\int_{-\infty}^{\infty} d\omega \int_{-\infty}^{\infty} dg'\, T\tilde{E}_z e^{i\omega t - ih_t' x' - ig' y'}, \tag{26}$$

where $\tilde{E}_z(g,\omega)$ is given by Eq. (6) (g should be expressed in terms of g' using the relations given above.) The reflected wave can be found from Eq. (26) by replacing $T \to R$ and $\exp(i\omega t - ih_t' x' - ig' y') \to \exp(i\omega t + ih_r' x' - ig' y')$.

V. TERAHERTZ SPECTRUM AND ENERGY FOR $LINBO_3$ AT 10 K AND 300 K

A. Spectral-spatial distribution of terahertz emission from the crystal

To find the total terahertz energy emitted per unit area of the exit boundary, i.e., the terahertz fluence, we integrate the x'-component of the Poynting vector $S_{x'}$ in vacuum (at $x' = 0+$) over infinite interval of time ($-\infty < t < \infty$). To find $S_{x'} = -c(4\pi)^{-1} E_z B_{y'}$, we use the relation between the Fourier components of the electric and magnetic fields in vacuum $\tilde{B}_{y'} = -ch_t'(\omega\cos\alpha)^{-1}\tilde{E}_z$ and the inverse transform of $\tilde{B}_{y'}$. On integrating $S_{x'}$, we obtain the fluence

$$\Phi(y') = \int_0^{\infty} d\omega \Phi_\omega(\omega, y'), \tag{27}$$

where the spectral density of fluence is

$$\Phi_\omega(\omega,y') = \frac{c^2}{\cos^2\alpha}\int_{-\infty}^{\infty} dg' \int_{-\infty}^{\infty} dg'' e^{-i(g'+g'')y'} \frac{\mathrm{Re}\, h_t'}{\omega} \times T(\omega,g')T(-\omega,g'')\tilde{E}_z(\omega,g')\tilde{E}_z(-\omega,g'') \tag{28}$$

(Re denotes taking the real part).

Figure 5 shows the distributions $\Phi_\omega(\omega,y')$ (2D graphs) and $\Phi(y')$ (1D graphs at the top of each panel) for different tilt angles and two damping rates (at two temperatures).

For 10 K and $\alpha = 62°$ [Fig. 5(a)], the terahertz fluence $\Phi(y')$ is provided by the near field of the nonlinear source (in the region $-1\ \mathrm{mm} \le y' \le 1\ \mathrm{mm}$) and the Cherenkov cone (at $y' > 1$ mm). For the near field ($-1\ \mathrm{mm} \le y' \le 1\ \mathrm{mm}$), the spectral density of fluence $\Phi_\omega(\omega,y')$ extends up to 2 THz and reaches a maximum at $\omega \approx 0.4$ THz. For the Cherenkov cone ($y' > 1$ mm), the spectrum is narrower and concentrated around 0.3 THz, in agreement with the formula $\omega\tau_- = \sqrt{2}$ (see Sec. III D). For $\alpha = 62°$ and 300 K, the distributions $\Phi_\omega(\omega,y')$ and $\Phi(y')$ (not shown) are similar to Fig. 5(a). The only difference is in the rate of fading of the fluence component $\Phi(y')$, which is related to the Cherenkov cone, with y': it fades much more rapidly at 300 K than at 10 K.

For 10 K and $\alpha = 64.4°$ [Fig. 5(b)], the maximal fluence is almost two orders of magnitude larger than in Fig. 5(a). The generated terahertz energy is provided mainly by the phase-matched wave as evidenced by the maximum of the spectral density of fluence at the phase-matched frequency of 1.5 THz given by Eq. (11). Since the interval of y' which has significant values of $\Phi_\omega(\omega,y')$ is shifted to larger y' from the region where the optical pulse exists ($-1\ \mathrm{mm} \le y' \le 1\ \mathrm{mm}$), the near field practically does not contribute to the terahertz yield. Additionally, the Cherenkov cone with central frequency of 1.3 THz in Fig. 5(b) is weak

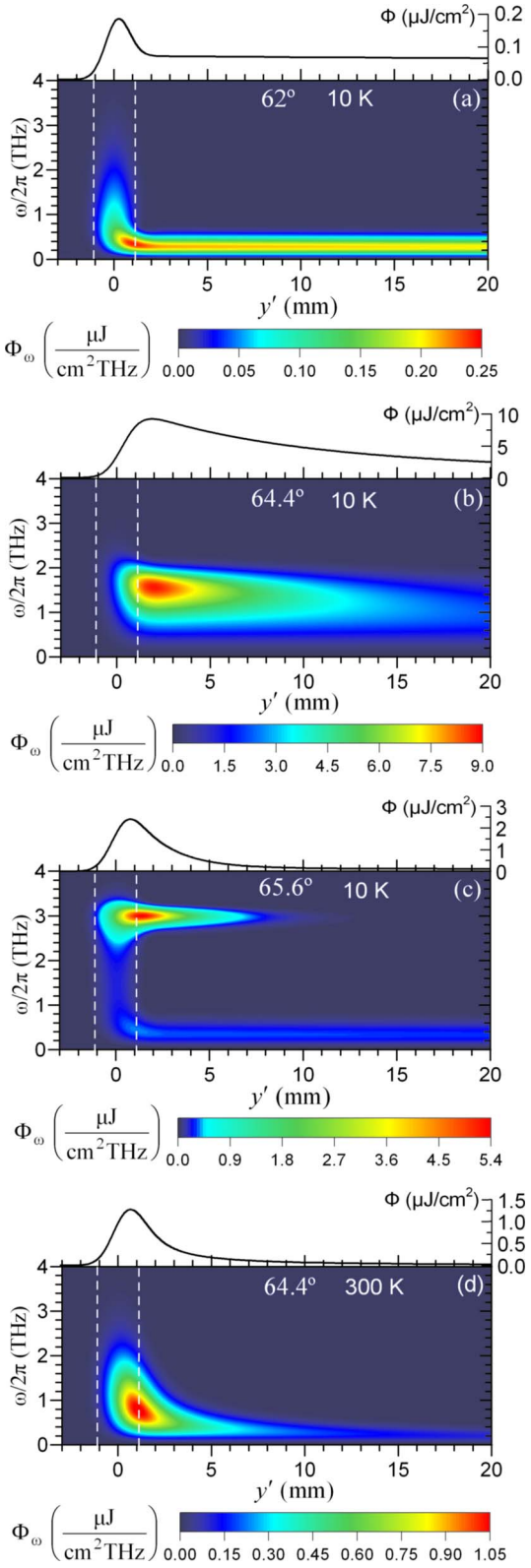

FIG. 5. (Color online) The distributions $\Phi_\omega(\omega,y')$ and $\Phi(y')$ for the $LiNbO_3$ crystal excited with Ti:sapphire laser ($\tau_{FWHM} = 150$ fs, $\ell_{\perp FWHM} = 1$ mm, and $I_0 = 10$ GW/cm^2). The temperature and α are shown on the panels. The interval of y', where the optical pulse exists, is marked (at the half-maximum level) by dashed lines.

compared to the phase-matched wave. The dominating role of the phase-matched wave for 10 K and $\alpha \gtrsim \alpha_{\min}$ is especially clear from Fig. 5(c), where the contributions from the phase-matched wave [with $\omega_0 \approx 3$ THz, see Eq. (11)] and the Cherenkov cone (with $\omega \approx 0.2$ THz) are well separated.

For 300 K and $\alpha = 64.4°$ [Fig. 5(d)], the maximal fluence is almost an order of magnitude smaller than in Fig. 5(b). The terahertz energy is provided mainly by the near field and the Cherenkov cone; the phase-matched wave at $\omega_0 \approx 0.9$ THz, see Eq. (11), is practically not excited. The contributions of these three terms into $\Phi_\omega(\omega, y')$ at its maximum around $y' \sim 1$ mm cannot be easily separated on Fig. 5(d). However, the distributions $\Phi_\omega(\omega, y')$ and $\Phi(y')$ for 300 K and $\alpha = 65.6°$ (not shown) are very similar to Fig. 5(d) demonstrating no contribution from the phase-matched wave with $\omega_0 \approx 2.8$ THz.

Figure 5 allows one to estimate the terahertz energy W emitted from the crystal (per unit length of the line source) as the area under the curve $\Phi(y')$. Since we are interested in generating frequencies ≥ 0.5 THz, we do not consider Fig. 5(a), where the main part of the generated spectrum lies well below 0.5 THz, and will omit the low-frequency Cherenkov tails in $\Phi(y')$ in Figs. 5(c) and 5(d). For 300 K and $\alpha = 64.4°$ [Fig. 5(d)], we obtain $W \sim 0.3$ μJ/cm. Normalization to the optical pulse energy $W_0 \approx 170$ μJ/cm (inside the crystal per unit length of the z-axis) gives a conversion efficiency of $W/W_0 \sim 2 \times 10^{-3}$. This value is higher by a factor of ~ 20 than the experimental data of Ref. 14 for the same optical intensity. A possible reason for this discrepancy is the use of the one-resonance model (1) for terahertz absorption at 300 K. We will develop a more accurate model and compare its results with the experimental data for 300 K in more detail in Sec. V C.

For 10 K and $\alpha = 65.6°$, we obtain from Fig. 5(c) $W \sim 0.9$ μJ/cm and $W/W_0 \sim 5 \times 10^{-3}$. For 10 K and $\alpha = 64.4°$ [Fig. 5(b)], the terahertz energy is estimated as $W \sim 15$–17 μJ/cm, depending on the width $(0 < y' < 20$–30 mm) of integration interval for $\Phi(y')$. The conversion efficiency is $W/W_0 \sim 10^{-1}$. It should be emphasized that to achieve such high efficiency one needs to use large crystals with dimensions of a few centimeters. In Ref. 4, the experimentally measured dependence $W(\alpha)$ for 10 K is in arbitrary units and, thus, cannot be compared directly with our predictions. In Ref. 18, the calculated terahertz energy is also given in arbitrary units and a tenfold increase in the generated terahertz energy is predicted when cooling the crystal from room temperature to 10 K. According to our estimates given above, the increase may be significantly higher (~ 50 times).

B. Optimizing parameters for 10 K

Let us study now how the generated terahertz spectrum and energy depend on $\ell_\perp$ and τ, and define the parameters maximizing the terahertz yield. We start with cryogenically cooled $LiNbO_3$. By integrating $\Phi_\omega(\omega, y')$ given by Eq. (28) over $-\infty < y' < \infty$, we obtain the spectral density of emitted terahertz energy

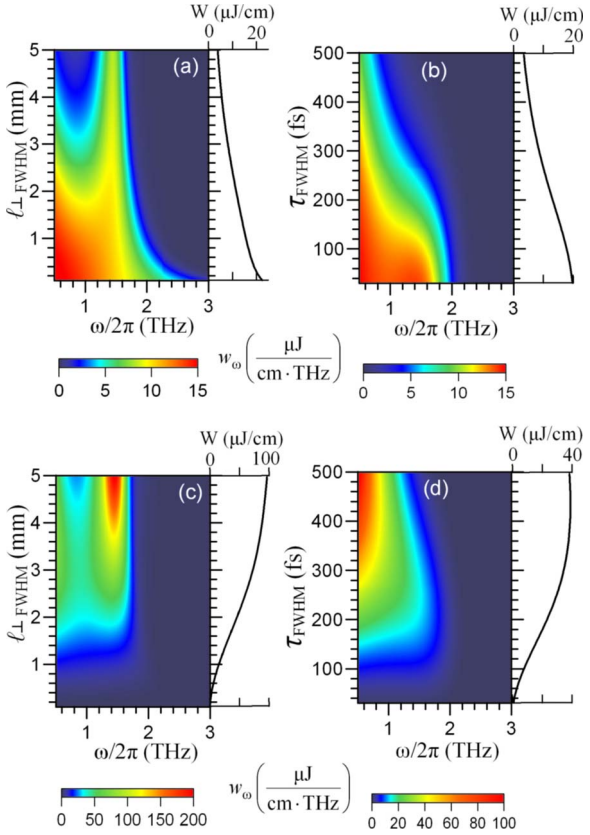

FIG. 6. (Color online) The spectral density of the terahertz energy $w_\omega(\omega)$ in dependence on $\ell_{\perp\mathrm{FWHM}}$ [(a) and (c)] and τ_{FWHM} [(b) and (d)] at 10 K and $\alpha = 64.4°$ for [(a) and (b)] the fixed energy (170 μJ/cm) and [(c) and (d)] fixed intensity (10 GW/cm^2) of the optical pulse. At the right sides of the panels, the terahertz energy W is shown as a function of $\ell_{\perp\mathrm{FWHM}}$ [(a) and (c)] and τ_{FWHM} [(b) and (d)]. In (a) and (c) $\tau_{\mathrm{FWHM}} = 150$ fs, in (b) and (d) $\ell_{\perp\mathrm{FWHM}} = 1$ mm.

$$w_\omega(\omega) = \frac{2\pi c^2}{\cos^2\alpha} \int_{-\infty}^{\infty} dg' \frac{\mathrm{Re}\ h_t'}{\omega} |T(\omega, g')|^2 |\tilde{E}_z(\omega, g')|^2. \tag{29}$$

Figure 6 shows w_ω as a function of ω [0.5 THz $< \omega/(2\pi) < 4$ THz], $\ell_{\perp\mathrm{FWHM}}$, and τ_{FWHM} for 10 K. In Fig. 6, we plotted also the total terahertz energy (per unit length of the line source)

$$W = \int d\omega w_\omega(\omega) \tag{30}$$

[the integral is taken over the interval 0.5 THz $< \omega/(2\pi) < 4$ THz] as a function of $\ell_{\perp\mathrm{FWHM}}$ and τ_{FWHM}.

For a fixed energy of the optical pulse [Figs. 6(a) and 6(b)], the total terahertz energy W increases with decreasing both $\ell_{\perp\mathrm{FWHM}}$ [Fig. 6(a)] and τ_{FWHM} [Fig. 6(b)]. Despite similar functions $W(\ell_{\perp\mathrm{FWHM}})$ and $W(\tau_{\mathrm{FWHM}})$, $\ell_{\perp\mathrm{FWHM}}$ and τ_{FWHM} affect the spectrum $w_\omega(\omega)$ in a different way. At large $\ell_{\perp\mathrm{FWHM}}$ the phase-matched frequency $\omega_0 \approx 1.5$ THz dominates in the spectrum [Fig. 6(a)]; with decreasing $\ell_{\perp\mathrm{FWHM}}$ the value $w_\omega(\omega_0)$ grows but slower than $w_\omega(\omega)$ at the frequencies $\omega < \omega_0$ corresponding to the near field and the Cherenkov cone—for $\ell_{\perp\mathrm{FWHM}} < 1$ mm the frequencies $\omega/(2\pi) \leq 1$ THz become dominating in the spectrum. At large τ_{FWHM}, the phase-matched wave is practically not ex-

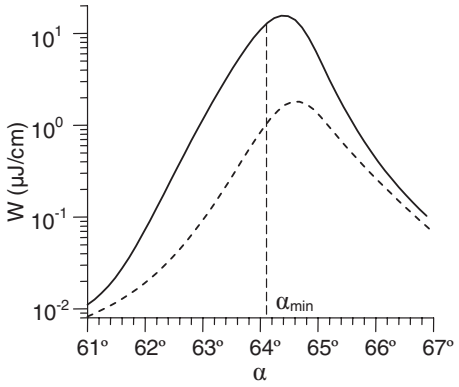

FIG. 7. The terahertz energy W as a function of α at 10 K for $\ell_{\perp\mathrm{FWHM}}=1$ mm and $\tau_{\mathrm{FWHM}}=150$ fs. The dashed curve shows the energy passed through the interval $-0.5\ \mathrm{mm}<y'<2\ \mathrm{mm}$.

cited and the low-frequency Cherenkov cone dominates in the spectrum; $w_\omega(\omega_0)$ grows with decreasing τ_{FWHM} and for $\tau_{\mathrm{FWHM}}<150$ fs becomes of the same order of magnitude as the low-frequency Cherenkov part of the spectrum [Fig. 6(b)].

For a fixed optical intensity [Figs. 6(c) and 6(d)], W grows with increasing $\ell_{\perp\mathrm{FWHM}}$ and the phase-matched frequency ω_0 becomes dominating in the spectrum $w_\omega(\omega)$ [Fig. 6(c)]. The dependence of W on τ_{FWHM} is similar to the dependence on $\ell_{\perp\mathrm{FWHM}}$. However, the excitation of the phase-matched wave becomes most efficient when $180\ \mathrm{fs}<\tau_{\mathrm{FWHM}}<320$ fs [Fig. 6(d)].

Figure 7 shows the dependence $W(\alpha)$ at 10 K calculated using Eqs. (29) and (30). This dependence with characteristic maximum near $\alpha_{\min}$ agrees qualitatively with the experimental curve from Ref. 4. Unfortunately, a quantitative comparison is impeded by arbitrary units used in Ref. 4. $A\sim 2°$-difference in the position of the curve maximum can be explained by the fact that ε_0 we used (see Sec. III A) was not fitted exactly to the material of Ref. 4 [see Eq. (9)]. Two interesting features can be seen in Fig. 7. First, the dependence $W(\alpha)$ is asymmetric with respect to $\alpha_{\min}$. Its maximum is shifted to larger α. This is explained by the excitation of the phase-matched wave at $\alpha>\alpha_{\min}$. There is no such excitation at $\alpha<\alpha_{\min}$. When α approaches $\alpha_{\min}$ from below, W grows due to enhancement of the near field [see Eq. (10)] and the field on the Cherenkov cone [see Eq. (18)]. After α passes through $\alpha_{\min}$, these fields begin to decrease but W continues to grow due to the excitation of the phase-matched wave. Further growth of α results in a decrease in the terahertz energy due to reduction in the amplitude of the phase-matched wave (see Fig. 3). The second feature is an order of magnitude decrease in the maximum value of the generated terahertz energy as the crystal becomes smaller. This is demonstrated by integrating the terahertz energy over $-0.5\ \mathrm{mm}<y'<2$ mm (see Fig. 7). Taking such a small interval is equivalent to using small crystals (with dimensions of ~ 2 mm) in experiments in Refs. 4 and 14.

C. Optimizing parameters for 300 K

At room temperature, the experimentally measured terahertz absorption coefficient in $LiNbO_3$ (see Ref. 21) has a more complicated frequency dependence than it is given by the one-resonance model (1). In the experiments, the absorption drops slower with frequency decrease below 2 THz as compared to the one-resonance model. This leads to a more rapid fading of the terahertz field at the Cherenkov cone than predicted by Eq. (21). Moreover, the terahertz absorption significantly differs for congruent and stoichiometric $LiNbO_3$ crystals and depends on Mg-doping level.[21] To obtain results that are more adequate to the experiments in Refs. 4 and 14 at 300 K and to study how the model of absorption affects the generated terahertz spectrum and energy, we performed calculations using a more realistic model of terahertz absorption for 0.68 mol % stoichiometric $LiNbO_3$ with parameters taken from Ref. 21. The calculations of Ref. 18 were also done for this material.

In our calculations, the experimentally measured frequency dependence of the amplitude absorption coefficient β given in Ref. 21 was fitted with a polynomial $\beta[\mathrm{cm}^{-1}]=24.83-12.68\nu+15.91\nu^2$, where ν is expressed in terahertz. For the terahertz refractive index n_{THz} we used the fitting formula from Ref. 21: $n_{\mathrm{THz}}(\nu)=4.94+2.1\times10^{-2}\nu^2+1.2\times10^{-3}\nu^4$ with ν in terahertz. Although the experimental results in Ref. 21 were obtained for the frequency interval from 0.9 to ~ 4 THz, we extrapolated the polynomial fitting down to 0.5 THz. The applicability of such monotonic extrapolation is confirmed by the experimental results in Ref. 29.

Figure 8 shows w_ω as a function of ω ($0.5\ \mathrm{THz}<\omega/2\pi<4$ THz) and α for different $\ell_\perp$ and τ. In Fig. 8, we plotted also the total terahertz energy (per unit length of the line source) given by Eq. (30) as a function of α. Three conclusions can be drawn from Fig. 8. First, w_ω has a maximum at $\alpha_m\approx 63.5°$ and $\omega_m\approx 1-1.4$ THz. The value of ω_m slightly increases with decreasing $\ell_\perp$ and τ. The total energy W also reaches a maximum at $\alpha_m\approx 63.5°$ for all $\ell_\perp$ and τ. Second, the width of the curve $W(\alpha)$ is practically independent of τ and increases with decreasing $\ell_\perp$. The latter can be readily explained: with decreasing $\ell_\perp$ the source reduces to a point and, therefore, tilting the front becomes irrelevant. Third, the spectrum $w_\omega(\omega)$ changes with α similarly for different $\ell_\perp$ and τ if $\alpha<\alpha_m$ and differently if $\alpha>\alpha_m$. For $\alpha<\alpha_m$, the maximum of $w_\omega(\omega)$ moves to lower frequencies and its magnitude decreases with decreasing α, the shape of the spectrum does not change noticeably. For $\alpha>\alpha_m$, one can observe a similar behavior of $w_\omega(\omega)$ with increasing α in Figs. 8(b) and 8(c). In Figs. 8(a) and 8(d), the spectrum $w_\omega(\omega)$ broadens with α.

Figure 9 shows the conversion efficiency as a function of $\ell_{\perp\mathrm{FWHM}}$ and τ_{FWHM} for $\alpha=63.5°$. For a fixed energy of the optical pulse [Fig. 9(a)], the efficiency grows with decreasing $\ell_{\perp\mathrm{FWHM}}$ and τ_{FWHM}. This growth is natural due to increasing optical intensity. The saturation of the growth at small τ_{FWHM} agrees with the predictions of Secs. III C and III D. For $\ell_{\perp\mathrm{FWHM}}=1$ mm and $\tau_{\mathrm{FWHM}}=150$ fs, Fig. 9(a) gives an efficiency of $\sim 7\times10^{-4}$, that is approximately three times smaller than the estimation made in Sec. V A on the basis of the one-resonance model. The value $\sim 7\times10^{-4}$ is still approximately seven times greater than the experimental data of Ref. 14. To obtain a better agreement with the

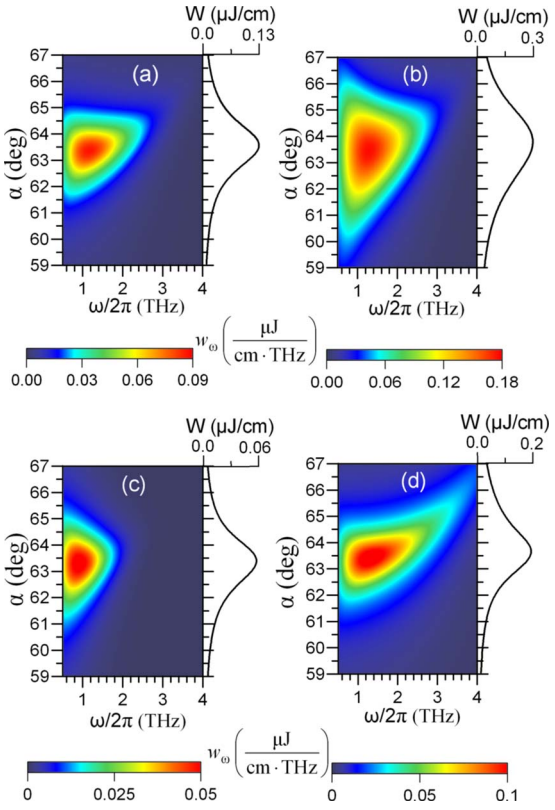

FIG. 8. (Color online) The spectral density of the terahertz energy w_ω as a function of ω and α at 300 K for different parameters of the optical pulse: $\ell_{\perp FWHM}=1$ mm, $\tau_{FWHM}=150$ fs (a), $\ell_{\perp FWHM}=0.3$ mm, $\tau_{FWHM}=150$ fs (b), $\ell_{\perp FWHM}=1$ mm, $\tau_{FWHM}=300$ fs (c), and $\ell_{\perp FWHM}=1$ mm, $\tau_{FWHM}=50$ fs (d). At the right sides of the panels, the terahertz energy W is shown as a function of α. The optical pulse energy is fixed to 170 μJ/cm.

experiment,[14] two additional factors should be taken into account. First, we calculated the efficiency as a ratio of the generated terahertz energy to the energy of the optical pulse in the crystal, thus, implying the optimal situation when the optical reflection at the entrance boundary of the crystal is suppressed by an antireflective coating. Such a coating was not used in Ref. 14, therefore, the optical intensity in the crystal was ~0.87 of the intensity of the incident laser pulse in vacuum. This reduces the efficiency by a factor of

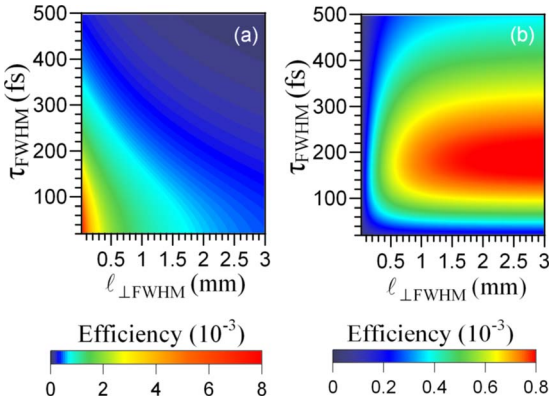

FIG. 9. (Color online) The optical-to-terahertz conversion efficiency as a function of $\ell_{\perp FWHM}$ and τ_{FWHM} at 300 K for the fixed optical pulse energy (170 μJ/cm) (a) and fixed optical intensity (10 GW/cm^2) (b). The tilt angle is $\alpha=63.5°$.

$\sim(0.87)^2\approx0.75$. Second, in the experiment[14] the optical intensity had a Gaussian-like profile along the z-axis. Since the terahertz fluence is proportional to the square of the optical intensity, its z-profile should be more narrow (by a factor of $1/\sqrt{2}\approx0.7$ for a Gaussian profile) than the optical intensity profile. This reduces the ratio of the terahertz/optical energies, i.e., the conversion efficiency, by a factor of ~0.7 comparing to our 2D case with a uniform distribution of the optical intensity along the z-axis. Thus, applying both of the above-mentioned factors we arrive at an estimated efficiency of $\sim4\times10^{-4}$ which is closer to that in Ref. 14.

For a fixed optical intensity [Fig. 9(b)], two interesting conclusions can be made. First, there is an optimal interval of $\tau_{FWHM}\sim150-250$ fs maximizing the efficiency. Second, the efficiency grows with $\ell_{\perp FWHM}$ while $\ell_{\perp FWHM}\leq1.5$ mm and saturates for $\ell_{\perp FWHM}>1.5$ mm. The saturation means that the generated terahertz energy scales linearly with the transverse size of the optical pulse in accord with the planar source approximation (see Sec. III C).

VI. CONCLUSION

To conclude, we have developed a theory that describes terahertz generation via optical rectification of femtosecond laser pulses with tilted intensity front in an electro-optic crystal. Our theory is based on a rigorous solution of Maxwell's equations with a source given by the moving nonlinear polarization excited by the pump. The pump is assumed to be 2D and, therefore, all effects related to the special (tilted) pulse geometry and finite transverse size are taken into account.

The general formulas that we derived include the parameters of the pump optical pulse (width, duration, tilt angle, group velocity) as well as the material properties (dispersion and absorption of the terahertz waves in the crystal). Using these formulas, we studied two situations of practical interest: $LiNbO_3$ excited with Ti:sapphire laser at room (300 K) and cryogenic (10 K) temperatures. We have studied the structure of the radiated fields inside the crystal and analyzed the spectral-spatial distribution of the terahertz emission from the crystal. It was shown that the contribution to the terahertz energy from the Cherenkov cone and the near field may be comparable to or even greater than the contribution from the phase-matched wave. This result cannot be obtained within the simple 1D model of Refs. 4 and 18. Our theoretical predictions agree well with the experimental data of Refs. 4 and 14. Our specific recommendations on achieving efficient terahertz generation with tilted-front pulses can be summarized briefly in the following way.

For 10 K, the crystal width and thickness should be ≥1 cm. The tilt angle α should be chosen in the interval of $\sim1°-2°$ near α_{min} ($\alpha_{min}\approx64.1°$ for $\varepsilon_0=26$), depending on required central frequency of the generated terahertz spectrum. For a fixed energy of the laser pulse, the parameters $\ell_{\perp FWHM}$ and τ_{FWHM} should be made as small as it is allowed by diffractive and dispersive broadening of the laser pulse and higher-order nonlinear effects that were neglected in our theory. For a fixed optical intensity (for example, just below the damage threshold of the crystal), it is advantageous to

increase $\ell_{\perp \mathrm{FWHM}}$; at the same time there is an interval of optimal durations τ_{FWHM} for the excitation of the phase-matched wave, for example, 180 fs $< \tau_{\mathrm{FWHM}} <$ 320 fs for the excitation of a 1.5 THz wave.

For 300 K, it is useless to increase the crystal width and thickness above ~5 mm. For 0.68 mol % stoichiometric $LiNbO_3$, the optimal tilt angle lies in the interval of 62.5°–64.5° depending on the required terahertz spectrum. For a fixed energy of the laser pulse, tight focusing to $\ell_{\perp \mathrm{FWHM}} \leq 100$ μm and compressing the pulse to $\tau_{\mathrm{FWHM}} < 150$ fs are preferable. For a fixed optical intensity, there is an interval of optimal durations τ_{FWHM} ~150–250 fs maximizing the conversion efficiency; the laser transverse size $\ell_{\perp \mathrm{FWHM}}$ should exceed 1.5 mm to provide the saturation of the efficiency and, thus, linear scaling of the generated terahertz energy with $\ell_{\perp \mathrm{FWHM}}$.

ACKNOWLEDGMENTS

We are grateful to Dr. A. V. Maslov for fruitful discussions. Two of the authors (M.I.B. and S.B.B.) were supported in part by the RFBR Grant No. 08-02-00988 and the RF President Grant No. MK-3749.2008.2. S.B.B. also acknowledges partial support from the fund "Dynasty."

[1] T. E. Stevens, J. K. Wahlstrand, J. Kuhl, and R. Merlin, Science **291**, 627 (2001).
[2] J. K. Wahlstrand and R. Merlin, Phys. Rev. B **68**, 054301 (2003).
[3] M. I. Bakunov, S. B. Bodrov, A. V. Maslov, and M. Hangyo, Phys. Rev. B **76**, 085346 (2007).
[4] J. Hebling, A. G. Stepanov, G. Almási, B. Bartal, and J. Kuhl, Appl. Phys. B: Lasers Opt. **78**, 593 (2004).
[5] D. H. Auston, Appl. Phys. Lett. **43**, 713 (1983).
[6] D. H. Auston, K. P. Cheung, J. A. Valdmanis, and D. A. Kleinman, Phys. Rev. Lett. **53**, 1555 (1984).
[7] D. A. Kleinman and D. H. Auston, IEEE J. Quantum Electron. **20**, 964 (1984).
[8] Y.-S. Lee, T. Meade, V. Perlin, H. Winful, T. B. Norris, and A. Galvanauskas, Appl. Phys. Lett. **76**, 2505 (2000).
[9] J. A. L'Huillier, G. Torosyan, M. Theuer, Y. Avetisyan, and R. Beigang, Appl. Phys. B: Lasers Opt. **86**, 185 (2007); **86**, 197 (2007).
[10] G. Imeshev, M. E. Fermann, K. L. Vodopyanov, M. M. Fejer, X. Yu, J. S. Harris, D. Bliss, and C. Lynch, Opt. Express **14**, 4439 (2006).
[11] Y.-S. Lee, W. C. Hurlbut, K. L. Vodopyanov, M. M. Fejer, and V. G. Kozlov, Appl. Phys. Lett. **89**, 181104 (2006).
[12] J. Hebling, G. Almási, I. Kozma, and J. Kuhl, Opt. Express **10**, 1161 (2002).
[13] A. G. Stepanov, J. Hebling, and J. Kuhl, Appl. Phys. Lett. **83**, 3000 (2003).
[14] A. G. Stepanov, J. Kuhl, I. Z. Kozma, E. Riedle, G. Almási, and J. Hebling, Opt. Express **13**, 5762 (2005).
[15] K. L. Yeh, M. C. Hoffman, J. Hebling, and K. A. Nelson, Appl. Phys. Lett. **90**, 171121 (2007).
[16] K. L. Yeh, J. Hebling, M. C. Hoffman, and K. A. Nelson, Opt. Commun. **281**, 3567 (2008).
[17] M. C. Hoffmann, K.-L. Yeh, J. Hebling, and K. A. Nelson, Opt. Express **15**, 11706 (2007).
[18] B. Bartal, I. Z. Kozma, A. G. Stepanov, G. Almási, J. Kuhl, E. Riedle, and J. Hebling, Appl. Phys. B: Lasers Opt. **86**, 419 (2007).
[19] M. I. Bakunov, A. V. Maslov, and S. B. Bodrov, Phys. Rev. Lett. **99**, 203904 (2007).
[20] A. V. Shuvaev, M. M. Nazarov, A. P. Shkurinov, and A. S. Chirkin, Radiophys. Quantum Electron. **50**, 922 (2007).
[21] L. Pálfalvi, J. Hebling, J. Kuhl, Á. Péter, and K. Polgár, J. Appl. Phys. **97**, 123505 (2005).
[22] J. Faure, J. van Tilborg, R. A. Kaindl, and W. P. Leemans, Opt. Quantum Electron. **36**, 681 (2004).
[23] Y. J. Ding, Opt. Lett. **29**, 2650 (2004).
[24] K. Wynne and J. J. Carey, Opt. Commun. **256**, 400 (2005).
[25] N. S. Stoyanov, T. Feurer, D. W. Ward, E. R. Statz, and K. A. Nelson, Opt. Express **12**, 2387 (2004).
[26] To convert the nonlinear coefficients d_{33} given in SI to cgs one should use following rule: $d(\mathrm{cm/CGSE}) = (3 \times 10^{-8}/4\pi) d(\mathrm{pm/V})$.
[27] M. I. Bakunov, A. V. Maslov, and S. B. Bodrov, J. Appl. Phys. **98**, 033101 (2005).
[28] M. I. Bakunov, A. V. Maslov, and S. B. Bodrov, Phys. Rev. B **72**, 195336 (2005).
[29] T. Qiu and M. Maier, Phys. Rev. B **56**, R5717 (1997).